

Rotational magnetocaloric effect of anisotropic giant spin systems

Christian Beckmann^a, Julian Ehrens^a, Jürgen Schnack^{a,*}

^a*Dept. of Physics, Bielefeld University, P.O. box 100131, D-33501 Bielefeld, Germany*

Abstract

The magnetocaloric effect, that consists of adiabatic temperature changes in a varying external magnetic field, appears not only when the amplitude is changed, but in cases of anisotropic magnetic materials also when the direction is varied. In this article we investigate the magnetocaloric effect theoretically for the archetypical single molecule magnets Fe₈ and Mn₁₂ that are rotated with respect to a magnetic field. We complement our calculations for equilibrium situations with investigations of the influence of non-equilibrium thermodynamic cycles.

Keywords: Molecular Magnetism, Giant-spin model, Magnetocalorics

PACS: 75.50.Xx, 75.10.Jm, 76.60.Es, 75.40.Gb

1. Introduction

Magnetocalorics is an important thermodynamic concept with many applications for instance in room-temperature or sub-kelvin cooling [1, 2, 3, 4, 5, 6, 7]. It rests to a large extend on the magnetocaloric effect (MCE) [8] which states that in adiabatic processes, i.e. processes with constant entropy, the temperature changes upon the variation of the external magnetic field. Nowadays's research efforts focus e.g. on new materials [9, 10, 11] or theoretical optimization of (molecular) magnetic materials [12, 13, 14, 15].

While the typical magnetocaloric process employs variations of the magnitude of the external field, some ideas focus on the effect of a rotation of the field or equivalently of the sample [16, 17, 18, 19]. A practical reason for

*corresponding author

Email address: jschnack@uni-bielefeld.de (Jürgen Schnack)

this approach is given by the fact that mechanical rotations of the sample can be performed much more quickly than field sweeps. However, the rotational magnetocaloric effect (rMCE) requires anisotropic magnetic materials [20, 21]. In this article we therefore discuss how single-molecule magnets (SMM) perform as cooling agents in the kelvin temperature region. These materials are usually known for two other effects: slow relaxation and quantum tunneling of the magnetization [22, 23, 24, 25] and not considered for magnetic cooling in the ordinary sense. Nevertheless, their large anisotropy makes them prospective candidates for the rMCE [18].

In this article we investigate two aspects of the rMCE. We first discuss the isentropes and isothermal entropy changes that can be achieved in SMMs such as Fe_8 and Mn_{12} . In a second part we set up a simple relaxation dynamics in order to estimate how more realistic time-dependent Carnot processes would perform for these molecular coolers.

The article is organized as follows. In section 2 we introduce the model. Section 3 deals with the equilibrium rotational magnetocaloric effect whereas section 4 discusses dynamical aspects. Our results are summarized in section 5.

2. Model and numerical procedures

2.1. Model Hamiltonians

The low-temperature properties of single-molecule magnets with a large spectral gap between the ground state multiplet and higher-lying states can be rationalized using the giant spin approximation. To this end the zero-field split ground state multiplet is generated by an effective one-spin Hamiltonian. For Fe_8 the following giant spin Hamiltonian was developed [25]

$$\begin{aligned} \tilde{H}_{\text{Fe}_8} = & D_{\text{Fe}_8} \tilde{S}_z^2 + E_{\text{Fe}_8} (\tilde{S}_x^2 - \tilde{S}_y^2) + g_{\text{Fe}_8} \mu_B \vec{B}(t) \cdot \vec{\tilde{S}} \\ & + B_{4,\text{Fe}_8}^0 \tilde{Q}_4^0 + B_{4,\text{Fe}_8}^2 \tilde{Q}_4^2 + B_{4,\text{Fe}_8}^4 \tilde{Q}_4^4, \end{aligned} \quad (1)$$

with specific values of $S = 10$, $D_{\text{Fe}_8} = -0.295$ K, $E_{\text{Fe}_8} = 0.05605$ K, $|E_{\text{Fe}_8}/D_{\text{Fe}_8}| = 0.19$, $B_{4,\text{Fe}_8}^0 = 2.3 \cdot 10^{-6}$ K, $B_{4,\text{Fe}_8}^2 = -7.2 \cdot 10^{-6}$ K, $B_{4,\text{Fe}_8}^4 = -1.2 \cdot 10^{-5}$ K, and $g_{\text{Fe}_8} = 2.0$ [26].

In the case of Mn_{12} , Hamiltonian (2) proved to be appropriate

$$\begin{aligned} \tilde{H}_{\text{Mn}_{12}} = & D_{\text{Mn}_{12}} \tilde{S}_z^2 + g_{\text{Mn}_{12}} \mu_B \vec{B}(t) \cdot \vec{\tilde{S}} \\ & + B_{4,\text{Mn}_{12}}^0 \tilde{Q}_4^0 + B_{4,\text{Mn}_{12}}^4 \tilde{Q}_4^4, \end{aligned} \quad (2)$$

with specific values of $S = 10$, $D_{\text{Mn}_{12}} = -0.65$ K, $B_{4,\text{Mn}_{12}}^0 = -3.0 \cdot 10^{-5}$ K, $B_{4,\text{Mn}_{12}}^4 = \pm 4.6 \cdot 10^{-5}$ K, and $g_{\text{Mn}_{12}} = 2.0$ [27]. Higher order spin operators are expressed by means of Stevens operators

$$\mathcal{Q}_4^0 = 35\mathcal{S}_z^4 - [30S(S+1) - 25]\mathcal{S}_z^2 + 3S^2(S+1)^2 - 6S(S+1) \quad (3)$$

$$\begin{aligned} \mathcal{Q}_4^2 = & \frac{1}{4} \left[7\mathcal{S}_z^2 - S(S+1) - 5 \right] \left((\mathcal{S}^+)^2 + (\mathcal{S}^-)^2 \right) \\ & + \frac{1}{4} \left((\mathcal{S}^+)^2 + (\mathcal{S}^-)^2 \right) \left[7\mathcal{S}_z^2 - S(S+1) - 5 \right] \end{aligned} \quad (4)$$

$$\mathcal{Q}_4^4 = \frac{1}{2} \left((\mathcal{S}^+)^4 + (\mathcal{S}^-)^4 \right). \quad (5)$$

It turns out that for the magnetocaloric investigations of this article only the terms given in the respective first lines of eqs. (1) and (2) are relevant. The other terms, which determine the tunnel splitting, have a stark effect on the magnetization tunneling, but not on the thermal properties for the temperature and field ranges as well as orientations studied here. We therefore use only the first lines of (1) and (2) in the following calculations.

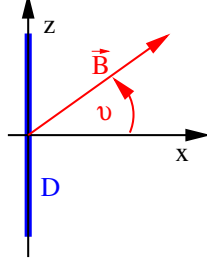


Figure 1: Coordinate system used in the simulations.

Since we are going to investigate the influence on the relative orientation of the magnetic field with respect to the easy axis of the SMM, we define the coordinate system as shown in Fig. 1. The magnetic easy axis is parallel to the z -axis, whereas the field vector lies in the xz -plane with an inclination of ϑ with the positive x -axis.

2.2. Equilibrium thermodynamics

Here and throughout the article we tacitly assume that the applied magnetic fields and the investigated temperatures do not violate the ranges of applicability of the giant spin models (1) and (2).

Equilibrium thermodynamic observables can be obtained from the Gibbs potential $G(T, \vec{B})$

$$G(T, \vec{B}) = -k_B T \log [Z(T, \vec{B})] , \quad (6)$$

where $Z(T, \vec{B})$ denotes the partition function. Entropy as well as magnetization are first derivatives of $G(T, \vec{B})$, i.e.

$$\mathcal{S}(T, \vec{B}) = -\frac{\partial}{\partial T} G(T, \vec{B}) , \quad (7)$$

$$\vec{\mathcal{M}}(T, \vec{B}) = -\frac{\partial}{\partial \vec{B}} G(T, \vec{B}) . \quad (8)$$

2.3. Non-equilibrium thermodynamics

The infinitesimal work δW is defined by the variation of the magnetization

$$\delta W = \vec{B} \cdot d\vec{\mathcal{M}} . \quad (9)$$

Since this term is complicated to evaluate we use the following relation:

$$\oint d(\vec{\mathcal{M}} \cdot \vec{B}) = 0 = \oint \vec{B} \cdot d\vec{\mathcal{M}} + \oint \vec{\mathcal{M}} \cdot d\vec{B} \quad (10)$$

$$\Rightarrow \Delta W = -\oint \vec{\mathcal{M}} \cdot d\vec{B} . \quad (11)$$

The magnetization $\vec{\mathcal{M}}$ can be obtained from the time-dependent density matrix. For the time evolution of the density matrix we employ

$$\frac{d}{dt} \rho_{\sim}(t) = -i [\tilde{H}, \rho_{\sim}(t)] + c \cdot \lambda \left(\rho_{\sim}^{(\text{eq})}(T, \vec{B}) - \rho_{\sim}(t) \right) , \quad (12)$$

with

$$\rho_{\sim}^{(\text{eq})}(T, \vec{B}) = \frac{1}{Z(T, \vec{B})} \sum_n |n\rangle e^{-\beta E_n} \langle n| , \quad (13)$$

where $\beta = (k_B T)^{-1}$. E_n and $|n\rangle$ denote the eigenvalues and the corresponding eigenvectors of the Hamiltonian. The factor c depends on the nature of the current stroke in the process. For an isothermal process $c = 1$, for an adiabatic (or isolated) process $c = 0$. The factor λ denotes the coupling

strength of the system to one of the heat reservoirs and can in principle be different for each heat bath.

The mean magnetization can easily be calculated from the density matrix:

$$\vec{\mathcal{M}}(t) = -g \mu_B \text{Tr} \left\{ \vec{S}_{\sim} \rho_{\sim}(t) \right\} . \quad (14)$$

For the mean work ΔW done on or by the system during one stroke in the time interval $[t_0, t_1]$ one finds with (11)

$$\Delta W = - \int_{t_0}^{t_1} \vec{\mathcal{M}}(t) \cdot \dot{\vec{B}}(t) dt . \quad (15)$$

The during this process absorbed or emitted amount of heat ΔQ can be obtained from the change of the mean energy $\langle \tilde{H} \rangle$ of the system via the rules of thermodynamics:

$$\langle \tilde{H} \rangle(t) = \text{Tr} \left\{ \tilde{H}(t) \rho_{\sim}(t) \right\} , \quad (16)$$

$$\Delta \langle \tilde{H} \rangle = \langle \tilde{H} \rangle(t_1) - \langle \tilde{H} \rangle(t_0) = \Delta Q + \Delta W . \quad (17)$$

3. Quasi-static MCE

Quasi-static (equilibrium) MCE investigates the thermodynamic functions (7) & (8) as given by (e.g.) the canonical ensemble. Of special interest are the isentropes, i.e. curves of constant entropy, whose slopes are the so-called cooling rates as well as the isothermal entropy changes – both figures of merit for MCE materials. Figure 2 shows the isentropes of Mn_{12} (left column) and Fe_8 (right column) for $B = 0.1$ T, $B = 1$ T, and $B = 2$ T from top to bottom. Since both systems are modeled with rather similar Hamiltonians, the graphs for these two SMMs do look very similar. The behavior can be rationalized as follows. For a given and not too large magnitude of the external magnetic field the energy spectrum resembles a tilted parabola for $\vartheta = \pi/2$ (l.h.s. of Fig. 3). In particular, the ground state is not degenerate. This situation changes towards $\vartheta = 0$ (r.h.s. of Fig. 3), where the two ground state levels are virtually degenerate. This means that all isentropes with $\mathcal{S}/k_B \leq \log 2$ head towards absolute zero at $\vartheta = 0$. In addition, the top panels of Fig. 2 display isentropes with $\mathcal{S}/k_B = 0.7 > \log 2$ that only exhibit local minima at $\vartheta = 0$. All plots are symmetric about $\vartheta = 0$.

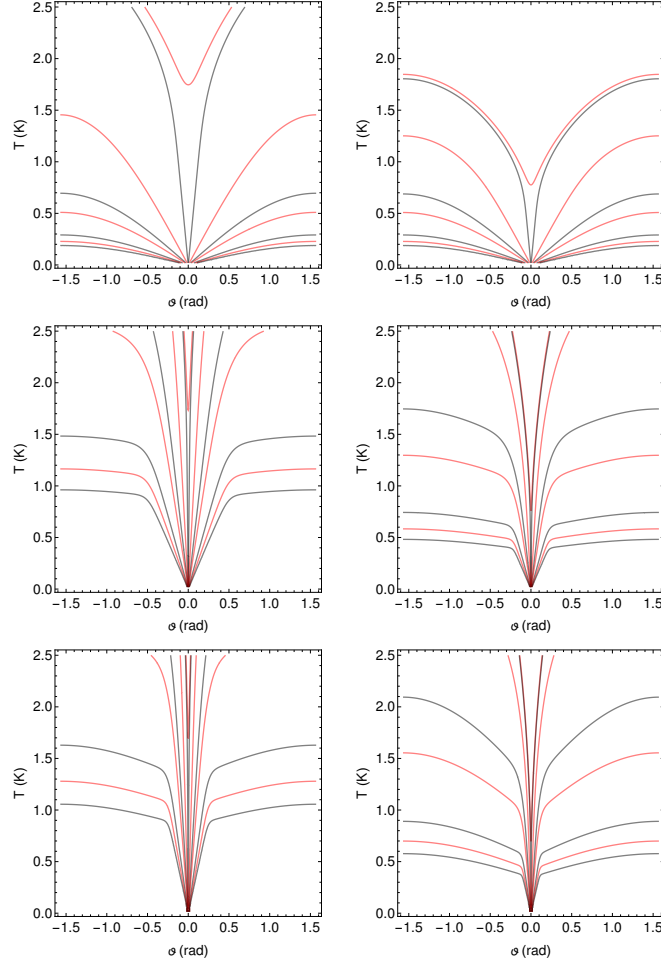


Figure 2: Isentropes of Mn_{12} (left column) and Fe_8 (right column) for $B = 0.1$ T, $B = 1$ T, and $B = 2$ T from top to bottom. Contours are drawn at entropy values S/k_B of 10^{-5} , 10^{-4} , 10^{-3} , 0.032, 0.1, 0.4, 0.68, and 0.7.

The cooling rate (slope of isentropes) assumes very large values close to $\vartheta = 0$. This trend increases with increasing magnitude of the applied field. Therefore, large temperature variations should be achievable with only mild rotations in particular for stronger fields.

The isothermal entropy change on the other hand is rather bounded since more than a twofold degeneracy of levels is not achievable in the physically permitted temperature and field ranges of the model. This leads to the characteristic curves displayed in Fig. 4. Shown is the negative entropy difference

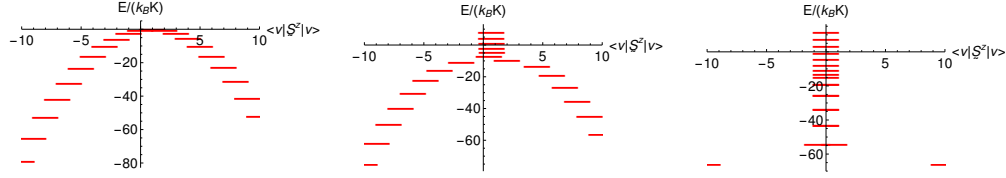


Figure 3: Energy eigenvalues vs. magnetization along z -direction for Mn_{12} at $B = 1$ T and $\vartheta = \pi/2$ (left), $\vartheta = \pi/4$ (middle), and $\vartheta = 0$ (right).

between final and initial orientation, i.e.

$$-\Delta\mathcal{S} = -(\mathcal{S}(T, B, \vartheta_f) - \mathcal{S}(T, B, \vartheta_i)) . \quad (18)$$

The initial angle is always taken as $\vartheta_i = 0$. The colors of the three curves in each panel correspond to the three chosen final angles ϑ_f displayed above the panels.

As one notices in all panels of Fig. 4 the isothermal entropy changes head for $\mathcal{S}/k_B = \log 2 \approx 0.68$ at low temperatures. This is a result of the twofold degeneracy at $\vartheta_i = 0$ and the vanishingly small entropy at all other angles $\vartheta_f \neq 0$. For elevated temperatures the entropy change rises a bit since then also higher lying levels are thermally populated. But due to the restricted number of levels, which are separated by gaps of the order of the anisotropy, this effect is small, albeit more pronounced for stronger external fields. The biggest entropy changes can be achieved by a rotation of $\Delta\vartheta = \pi/2$ from the direction perpendicular to the easy axis into the direction of the easy axis.

4. Realistic Carnot processes

A discussion of the magnetocaloric properties as in section 3 or many publications of the field rests on the assumption of thermal equilibrium, i.e. on idealized quasi-static processes. However, a realistic cooling experiment or Carnot process is executed on short time scales of e.g. minutes [6] or shorter. Whether the system stays close to equilibrium depends on its typical relaxation times. In addition, especially for small quantum systems, it is not granted that the isolated parts of the processes, where no thermal contact is established, are indeed adiabatic. They may as well be unitary which is not the same. We do not want to get into this very complicated discussion and therefore assume that the isolated steps of our processes are described by a unitary time evolution. This assumption appears further justified since we investigate only fast processes in the following. Investigations

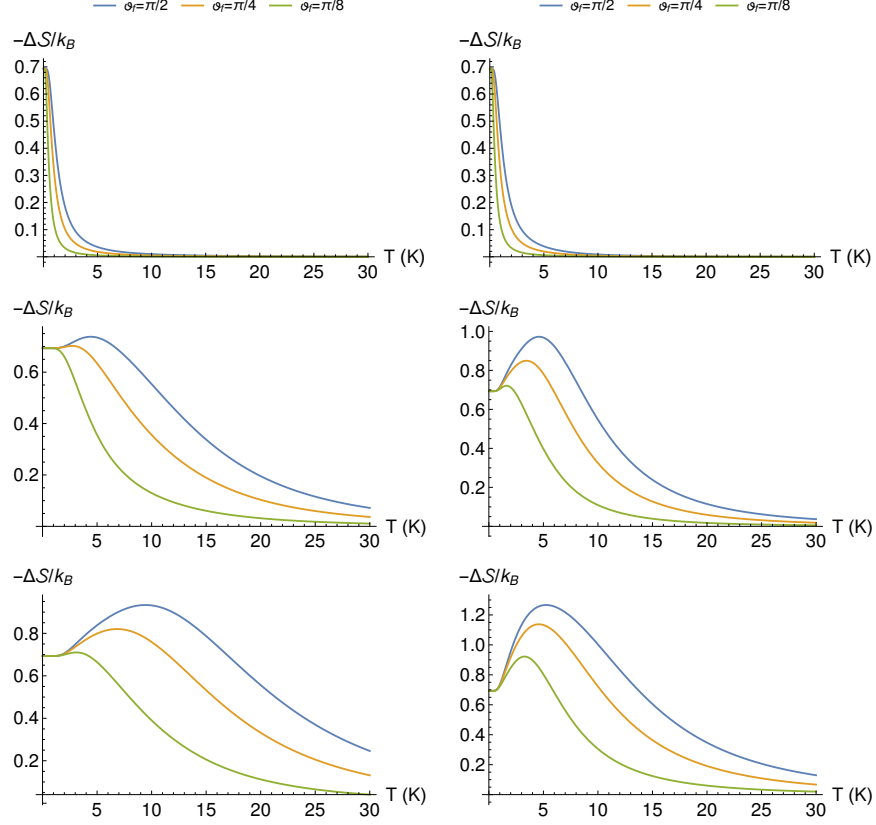


Figure 4: Isothermal entropy changes of Mn₁₂ (left column) and Fe₈ (right column) for $B = 0.1$ T, $B = 1$ T, and $B = 2$ T from top to bottom. The rotation is performed from the initial angle $\vartheta_i = 0$ to the final angles ϑ_f provided at the top.

of slower processes and processes other than Carnot are postponed to future investigations.

The Carnot process consists of two isothermal (strokes II and IV) and two isolated processes (strokes I and III). The time evolution of the medium, in our case a single Mn₁₂ SMM, is modeled via the time evolution of its density matrix according to (12). Although the cycle time τ_c is in reality only limited by the relaxation during the isothermal strokes, we choose for the sake of simplicity for all four strokes the same time duration. We choose $T_h = 0.65$ K as the temperature of the hot reservoir and $T_c = 0.5$ K as the temperature of the cold reservoir, respectively. For the coupling constant λ we choose $\lambda_h = \lambda_c = 10^{-1}$ ps⁻¹. Smaller values of λ simply lead to a shift to

lower operating frequencies $f = \tau_c^{-1}$ and a rescaling of the observed power. Since we investigate the Carnot process in the realization as a refrigerator important quantities of interest are the cooling power P and the efficiency ϵ :

$$P = \frac{Q_c}{\tau_c}, \quad (19)$$

$$\epsilon = \frac{Q_c}{W}, \quad (20)$$

where Q_c is the amount of heat taken from the cold reservoir and W is the amount of work absorbed by the system during one complete cycle.

The time dependent angle $\vartheta(t)$ and the behavior of the coupling constant $c \cdot \lambda$ is exemplarily shown in Fig. 5 for a cycle time of $\tau_c = 20$ ns. Figure Fig. 5 also shows the process in the corresponding T - ϑ -diagram.

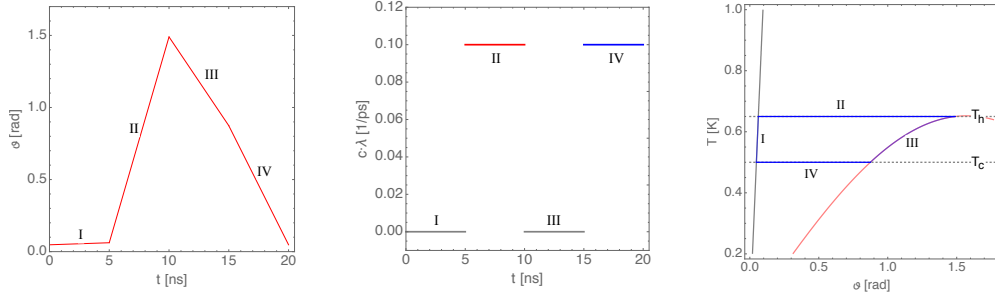


Figure 5: Exemplaric time dependence of the angle $\vartheta(t)$ (left hand side) and of the coupling constant $c \cdot \lambda$ (middle). The coupling to the hot reservoir λ_h is shown in red, the coupling to the cold reservoir λ_c is shown in blue. The right hand side shows an equilibrium, i.e. fully relaxed Carnot process in the T - ϑ -diagram.

During the beginning of stroke I the system is in thermal equilibrium with the cold heat reservoir at temperature T_c . The system is then decoupled from the heat reservoir and the angle ϑ is changed with constant angular velocity from ϑ_0 to ϑ_1 (compare stroke I in Fig. 5). Since the system evolves isolated during this stroke there is no heat exchanged with the reservoirs. The work can therefore be calculated via (17).

During stroke II the coupling to the hot heat reservoir is switched on while the angle ϑ is further increased to ϑ_2 with a constant (but different to the previous step) velocity (compare stroke II in Fig. 5). The system relaxes during this stroke towards thermal equilibrium with the hot heat reservoir, but depending on the time of contact with the bath, equilibrium

is not necessarily reached. Since this stroke is isothermal the work must be calculated via (15). The amount of heat Q_h exchanged with the hot heat reservoir can then be calculated via (17).

For stroke III the system is again decoupled from the heat reservoir and the angle ϑ is decreased with another constant velocity from ϑ_2 to ϑ_3 (compare stroke III in Fig. 5). Because this stroke is again isolated and there is again no heat exchange with any of the heat reservoirs the work can be calculated directly from (17).

During the last stroke IV the system is coupled to the cold heat reservoir at temperature T_c while the angle ϑ is decreased with another constant velocity until the initial angle ϑ_0 is reached and the cycle is complete (compare stroke IV in Fig. 5). The system evolves towards thermal equilibrium with the cold heat reservoir as much as possible during contact time. Since this stroke is again isothermal the work must be calculated via (15). The amount of heat Q_c exchanged with the cold heat reservoir can then be calculated from (17).

The observables presented in the following parts are evaluated after the system has been driven through sufficiently many cycles in order to reach a steady state.

4.1. Dependence of power and operating frequencies on the amplitude of $\vec{B}(t)$

At first we investigate the influence of the amplitude B_0 of the magnetic field $\vec{B}(t)$ on the maximum cooling power P , the optimal operating frequency f_{opt} , the efficiency ϵ_{opt} as well as on the maximum operating frequency f_{max} . Here the optimal operating frequency f_{opt} denotes the operating frequency and ϵ_{opt} the efficiency at maximum cooling power. The maximum operating frequency f_{max} is the maximal frequency for which the Carnot cycle works as a refrigerator delivering heat from the cold heat reservoir to the hot one by consuming work. The results of our simulations are shown in Fig. 6. The angles ϑ_0 to ϑ_3 are chosen such that the process always operates between the two isentropes $\mathcal{S}_{\text{max}}/k_B = 0.68$ and $\mathcal{S}_{\text{min}}/k_B = 0.032$ and therefore with a fixed $\Delta\mathcal{S}/k_B = 0.648$.

The minimal possible amplitude B_0 that can satisfy \mathcal{S}_{min} and \mathcal{S}_{max} at the given temperatures of the heat reservoirs is $B_0 = 0.128$ T. As one can deduce from Fig. 6, P , f_{opt} and f_{max} are maximal for this amplitude. Only the efficiency at maximum power ϵ_{opt} is minimal. When one increases the amplitude B_0 , P decreases by 7.66% until the amplitude B_0 reaches a threshold value of about 0.5 T. The optimal operating frequency f_{opt}

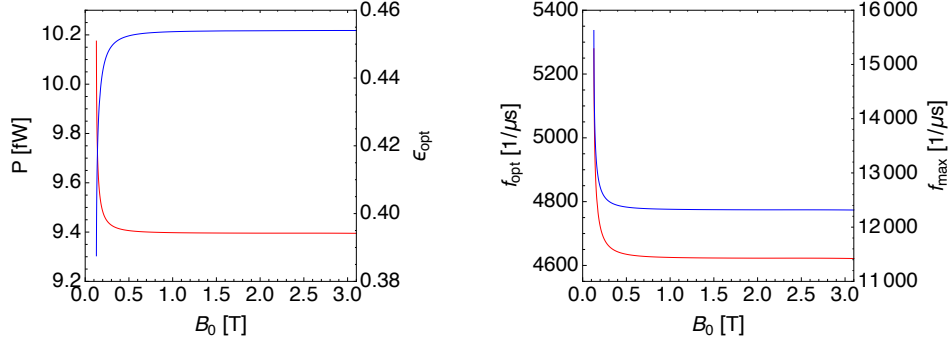


Figure 6: Dependence of the maximum cooling power P and corresponding efficiency ϵ_{opt} (left hand side) and the optimal and maximal operating frequency f (right hand side) on the amplitude of the magnetic field B_0 . The curves belonging to the left axis are shown in red, the curves belonging to the right axis are shown in blue. Different scales are used.

decreases in the same time by 12.45% and f_{max} decreases by even 21.17%. The efficiency on the other hand increases by 17.15%. For larger values of B_0 all observed quantities become independent of B_0 .

For the hot and cold temperatures T_c and T_h , respectively, chosen in our example, one also deduces from Fig. 2 that with increasing field strength B_0 the maximum rotation angle decreases. Therefore, for large amplitudes B_0 only very small rotations are necessary.

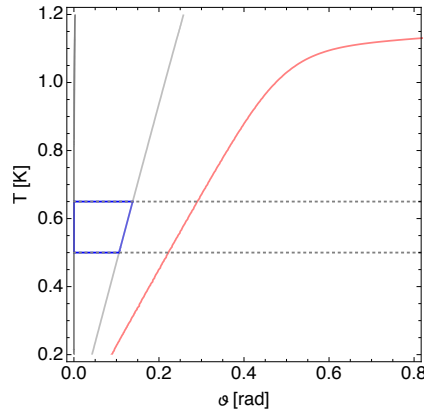


Figure 7: Exemplaric depiction of the Carnot cycle in the T - φ -diagram. The isentrope \mathcal{S}_{max} (black line) is fixed at $\mathcal{S}/k_B = 0.6931$ while the isentrope \mathcal{S}_{min} (gray line) is varied between black line and red curve to achieve different $\Delta\mathcal{S}$. The temperatures of the two heat reservoirs are marked by dotted gray lines. A Carnot cycle is depicted in blue.

4.2. Dependence of power and operating frequencies on $\Delta\mathcal{S}$

The quasi-static solution of the Carnot process yields a linear dependence between the heat extracted from the cold heat reservoir ΔQ_c and the entropy difference $\Delta\mathcal{S}$ between the two isentropes \mathcal{S}_{\min} and \mathcal{S}_{\max} of the process:

$$\Delta Q_c = T_c \cdot \Delta\mathcal{S}. \quad (21)$$

Thus a large value of $\Delta\mathcal{S}$ is intended to maximize the cooling per cycle. To investigate if this still holds for the dynamic process we investigate again the maximum cooling power P and the corresponding efficiency at maximum cooling power ϵ_{opt} as well as the operating frequencies f_{opt} and f_{max} . The amplitude B_0 of the applied magnetic field is fixed at $B_0 = 1$ T. We also fix the isentrope \mathcal{S}_{\max} to a value that is very close to the maximal possible value. We use $\mathcal{S}_{\max} = 0.6931 k_B$. The other isentrope \mathcal{S}_{\min} is varied to achieve different $\Delta\mathcal{S}$. This is exemplarily shown in Fig. 7.

The results of our simulations are shown in Fig. 8. As one can see from the left hand side of Fig. 8 the maximum cooling power P grows almost linearly with $\Delta\mathcal{S}$ (red curve). But there is a significant loss of P when $\Delta\mathcal{S}$ gets larger than $\Delta\mathcal{S}_{\text{opt}} = 0.668 k_B$ (that is 96.44% of the maximum value of $\Delta\mathcal{S}$). This loss is about almost 25% when the cycle is operated at maximum $\Delta\mathcal{S}$ instead of $\Delta\mathcal{S}_{\text{opt}}$. In contrast to the quasi-static case the largest $\Delta\mathcal{S}$ does not yield the maximum performance.

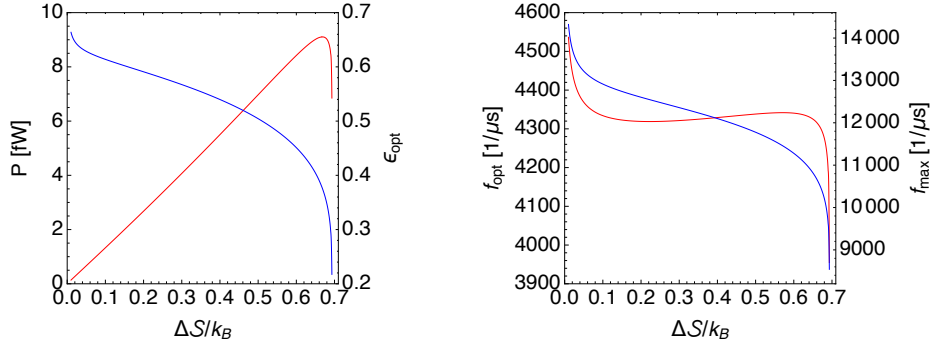


Figure 8: Dependence of the maximum cooling power P and corresponding efficiency ϵ (left hand side) and the optimal and maximal operating frequency f (right hand side) on the value of $\Delta\mathcal{S}$. The curves belonging to the left axis are shown in red, the curves belonging to the right axis are shown in blue. Different scales are used.

The efficiency ϵ_{opt} at maximum power decreases monotonically with growing $\Delta\mathcal{S}$ (blue curve in Fig. 8 l.h.s.), and the slope is larger for small as well as

large values of $\Delta\mathcal{S}$. The same is true for the maximum operating frequency f_{\max} (compare blue curve in Fig. 8 r.h.s.). The optimal operating frequency f_{opt} , red curve in Fig. 8 r.h.s., behaves differently, since it has a local minimum at $\Delta\mathcal{S} = 0.222 k_B$ (32.1% of the maximum $\Delta\mathcal{S}$) and a local maximum at $\Delta\mathcal{S} = 0.570 k_B$ (82.36% of the maximum $\Delta\mathcal{S}$).

5. Summary and outlook

In this article we report investigations of the rotational magnetocaloric effect using single molecule magnets. We can conclude that the effect is present and may be used in cases where quick field changes, that are possible using mechanical rotations, are necessary. The isothermal entropy change, on the other hand, is limited since degeneracies larger than two do not arise and thus the entropy does not grow much above $\mathcal{S}/k_B \approx \log 2$.

A description of the Carnot process as a realistic time-dependent non-equilibrium process – using a simplified dynamics – reveals that for SMMs a threshold field amplitude exists above which the characteristic figures do not change any more. In addition and in contrast to the quasi-static case the largest $\Delta\mathcal{S}$ does not yield the maximum performance. Instead the maximum cooling power is achieved with an optimal value for $\Delta\mathcal{S}$ of only about 96 % of the maximum possible value.

In future investigations slow processes shall be studied, where the interaction with the heat bath includes the relevant phonon degrees of freedom in order to take the phonon bottleneck into account [28, 29, 30, 31, 32].

Acknowledgment

The authors thank Wolfgang Wernsdorfer for useful discussions. Funding by the Deutsche Forschungsgemeinschaft (DFG SCHN 615/23-1) is thankfully acknowledged.

References

- [1] W. F. Giauque, D. MacDougall, Attainment of Temperatures below 1° Absolute by Demagnetization of $\text{Gd}_2(\text{SO}_4)_3 \cdot 8\text{H}_2\text{O}$, Phys. Rev. 43 (1933) 768, URL <https://link.aps.org/doi/10.1103/PhysRev.43.768>.

- [2] V. K. Pecharsky, K. A. Gschneidner, Magnetocaloric effect and magnetic refrigeration, *J. Magn. Mater.* 200 (1999) 44–56, URL <http://www.sciencedirect.com/science/article/pii/S0304885399003972>.
- [3] O. Waldmann, R. Koch, S. Schromm, P. Müller, I. Bernt, R. W. Saalfrank, Butterfly hysteresis loop at nonzero bias field in antiferromagnetic molecular rings: Cooling by adiabatic magnetization, *Phys. Rev. Lett.* 89 (2002) 246401.
- [4] M. Evangelisti, F. Luis, L. J. de Jongh, M. Affronte, Magnetothermal properties of molecule-based materials, *J. Mater. Chem.* 16 (2006) 2534–2549, URL <http://dx.doi.org/10.1039/B603738K>.
- [5] J. R. Gomez, R. F. Garcia, A. D. M. Catoira, M. R. Gomez, Magnetocaloric effect: A review of the thermodynamic cycles in magnetic refrigeration, *Renewable and Sustainable Energy Reviews* 17 (2013) 74 – 82, URL <http://www.sciencedirect.com/science/article/pii/S136403211200528X>.
- [6] J. W. Sharples, D. Collison, E. J. L. McInnes, J. Schnack, E. Palacios, M. Evangelisti, Quantum signatures of a molecular nanomagnet in direct magnetocaloric measurements, *Nat. Commun.* 5 (2014) 5321, URL <http://dx.doi.org/10.1038/ncomms6321>.
- [7] M. F. J. Boeije, P. Roy, F. Guillou, H. Yibole, X. F. Miao, L. Caron, D. Banerjee, N. H. van Dijk, R. A. de Groot, E. Brück, Efficient Room-Temperature Cooling with Magnets, *Chem. Mater.* 28 (14) (2016) 4901–4905, URL <https://doi.org/10.1021/acs.chemmater.6b00518>.
- [8] A. Smith, Who discovered the magnetocaloric effect?, *Eur. Phys. J. H* 38 (2013) 507–517, URL <http://dx.doi.org/10.1140/epjh/e2013-40001-9>.
- [9] N. T. Trung, L. Zhang, L. Caron, K. H. J. Buschow, E. Brück, Giant magnetocaloric effects by tailoring the phase transitions, *Appl. Phys. Lett.* 96 (17) (2010) 172504, URL <https://doi.org/10.1063/1.3399773>.

- [10] K. G. Sandeman, Magnetocaloric materials: The search for new systems, *Scripta Materialia* 67 (2012) 566 – 571, URL <http://www.sciencedirect.com/science/article/pii/S1359646212001595>.
- [11] A. Baniodeh, N. Magnani, Y. Lan, G. Buth, C. E. Anson, J. Richter, M. Affronte, J. Schnack, A. K. Powell, High spin cycles: topping the spin record for a single molecule verging on quantum criticality, *npj Quantum Materials* 3 (2018) 10, URL <https://doi.org/10.1038/s41535-018-0082-7>.
- [12] M. Evangelisti, E. K. Brechin, Recipes for enhanced molecular cooling, *Dalton Trans.* 39 (2010) 4672–4676, URL <http://dx.doi.org/10.1039/B926030G>.
- [13] E. Garlatti, S. Carretta, J. Schnack, G. Amoretti, P. Santini, Theoretical design of molecular nanomagnets for magnetic refrigeration, *Appl. Phys. Lett.* 103 (20) 202410, URL <http://scitation.aip.org/content/aip/journal/apl/103/20/10.1063/1.4830002>.
- [14] M. Evangelisti, G. Lorusso, E. Palacios, Comment on “Theoretical design of molecular nanomagnets for magnetic refrigeration” [*Appl. Phys. Lett.* 103, 202410 (2013)], *Applied Physics Letters* 105 (4) 046101, URL <http://scitation.aip.org/content/aip/journal/apl/105/4/10.1063/1.4891336>.
- [15] E. Garlatti, S. Carretta, J. Schnack, G. Amoretti, P. Santini, Response to Comment on Theoretical design of molecular nanomagnets for magnetic refrigeration [*Appl. Phys. Lett.* 105, 046101 (2014)], *Applied Physics Letters* 105 (4) 046102, URL <http://scitation.aip.org/content/aip/journal/apl/105/4/10.1063/1.4891337>.
- [16] G. Lorusso, O. Roubeau, M. Evangelisti, Rotating Magnetocaloric Effect in an Anisotropic Molecular Dimer, *Angew. Chem. Int. Ed.* 55 (2016) 3360–3363, URL <http://dx.doi.org/10.1002/anie.201510468>.
- [17] P. Konieczny, R. Peka, D. Czernia, R. Podgajny, Rotating Magnetocaloric Effect in an Anisotropic Two-Dimensional CuII[WV(CN)8]3 - Molecular Magnet with Topological Phase Transition: Experiment and Theory, *Inorganic Chemistry* 56 (19) (2017) 11971–11980, URL <http://dx.doi.org/10.1021/acs.inorgchem.7b01930>, pMID: 28915020.

- [18] F. Torres, J. M. Hernandez, X. Bohigas, J. Tejada, Giant and time-dependent magnetocaloric effect in high-spin molecular magnets, *Appl. Phys. Lett.* 77 (2000) 3248–3250, URL <http://dx.doi.org/10.1063/1.1325393>.
- [19] X. X. Zhang, H. L. Wei, Z. Q. Zhang, L. Zhang, Anisotropic Magnetocaloric Effect in Nanostructured Magnetic Clusters, *Phys. Rev. Lett.* 87 (2001) 157203, URL <https://link.aps.org/doi/10.1103/PhysRevLett.87.157203>.
- [20] V. Tkáč, R. Tarasenko, A. Orendáčová, M. Orendáč, V. Sechovský, A. Feher, Magnetocaloric effect and slow magnetic relaxation in $\text{CsGd}(\text{MoO}_4)_2$ induced by crystal-field anisotropy, *Physica B: Condensed Matter* (2017) in press, URL <http://www.sciencedirect.com/science/article/pii/S0921452617304982>.
- [21] R. Tarasenko, V. Tkáč, A. Orendáčová, M. Orendáč, A. Feher, Experimental study of the rotational magnetocaloric effect in $\text{KTm}(\text{MoO}_4)_2$, *Physica B: Condensed Matter* 538 (2018) 116 – 119, URL <http://www.sciencedirect.com/science/article/pii/S0921452618302199>.
- [22] R. Sessoli, D. Gatteschi, A. Caneschi, M. A. Novak, Magnetic bistability in a metal-ion cluster, *Nature* 365 (1993) 141–143, URL <http://dx.doi.org/10.1038/365141a0>.
- [23] J. R. Friedman, M. P. Sarachik, J. Tejada, R. Ziolo, Macroscopic Measurement of Resonant Magnetization Tunneling in High-Spin Molecules, *Phys. Rev. Lett.* 76 (1996) 3830–3833, URL <https://link.aps.org/doi/10.1103/PhysRevLett.76.3830>.
- [24] L. Thomas, F. Lioni, R. Ballou, D. Gatteschi, R. Sessoli, B. Barbara, Macroscopic quantum tunnelling of magnetization in a single crystal of nanomagnets, *Nature* 383 (1996) 145, URL <http://dx.doi.org/10.1038/383145a0>.
- [25] W. Wernsdorfer, R. Sessoli, Quantum Phase Interference and Parity Effects in Magnetic Molecular Clusters, *Science* 284 (1999) 133–135, URL <http://www.sciencemag.org/content/284/5411/133.abstract>.
- [26] A. L. Barra, D. Gatteschi, R. Sessoli, High-Frequency EPR Spectra of $[\text{Fe}_8\text{O}_2(\text{OH})_{12}(\text{tacn})_6]\text{Br}_8$: A Critical Appraisal of the Barrier for the

- Reorientation of the Magnetization in Single-Molecule Magnets, *Chem. Eur. J* 6 (2000) 1608–1614, URL [http://dx.doi.org/10.1002/\(SICI\)1521-3765\(20000502\)6:9<1608::AID-CHEM1608>3.0.CO;2-8](http://dx.doi.org/10.1002/(SICI)1521-3765(20000502)6:9<1608::AID-CHEM1608>3.0.CO;2-8).
- [27] E. d. Barco, A. D. Kent, S. Hill, J. M. North, N. S. Dalal, E. M. Rumberger, D. N. Hendrickson, N. Chakov, G. Christou, Magnetic Quantum Tunneling in the Single-Molecule Magnet Mn₁₂-Acetate, *J. Low Temp. Phys.* 140 (2005) 119–174, URL <https://doi.org/10.1007/s10909-005-6016-3>.
- [28] I. Chiorescu, W. Wernsdorfer, A. Müller, H. Bögge, B. Barbara, Butterfly hysteresis loop and dissipative spin reversal in the $S = 1/2$, V₁₅ molecular complex, *Phys. Rev. Lett.* 84 (2000) 3454–3457, URL <http://link.aps.org/doi/10.1103/PhysRevLett.84.3454>.
- [29] P. Santini, S. Carretta, E. Livioti, G. Amoretti, P. Carretta, M. Filibian, A. Lascialfari, E. Micotti, NMR as a probe of the relaxation of the magnetization in magnetic molecules, *Phys. Rev. Lett.* 94 (2005) 077203, URL <http://link.aps.org/doi/10.1103/PhysRevLett.94.077203>.
- [30] D. A. Garanin, Towards a microscopic understanding of the phonon bottleneck, *Phys. Rev. B* 75, URL <http://link.aps.org/abstract/PRB/v75/e094409>.
- [31] S. Carretta, T. Guidi, P. Santini, G. Amoretti, O. Pieper, B. Lake, J. van Slageren, F. E. Hallak, W. Wernsdorfer, H. Mutka, M. Russina, C. J. Milios, E. K. Brechin, Breakdown of the Giant Spin Model in the Magnetic Relaxation of the Mn₆ Nanomagnets, *Phys. Rev. Lett.* 100 (2008) 157203, URL <http://link.aps.org/abstract/PRL/v100/e157203>.
- [32] C. Beckmann, J. Schnack, Investigation of thermalization in giant-spin models by different Lindblad schemes, *J. Magn. Magn. Mater.* 437 (2017) 7–11, URL <http://www.sciencedirect.com/science/article/pii/S0304885316332139>.